On the Dynamics of Human Pilots in Marginally Controllable Systems

NORIHIRO GOTO*
Kyushu University, Fukuoka, Japan
AND
KYUICHIRO WASHIZU†
University of Tokyo, Tokyo, Japan

In designing V/STOL and high-speed flight vehicles, knowledge of the human pilot's controllability limit may be needed. Measurement of the pilot's describing function for his control of the system with marginal levels of static stability or damping, or both, is important to determine the controllability limit. This report includes the results of describing function measurement for dynamically or statically unstable second-order systems. Also included is a brief explanation of an improved time domain analysis method. When the system is dynamically unstable, the results show that the pilot employs a modified describing function that contains a second-order lead term with a particular time constant associated with the undamped natural frequency of the system. For the statically unstable case, the results indicate that the pilot pays attention only to the unstable first-order mode so that his describing function coincides with that for the first-order unstable system control.

Nomenclature

$G(s)$ = transfer function
K_p = pilot-adopted gain
T_L = pilot-adopted lead time constant
T_N = pilot neuromuscular lag time constant
X = damping
Y = static stability
$Y_c(s)$ = controlled element transfer function
$Y_p(s)$ = pilot transfer function
$c(t)$ = pilot output
$e(t)$ = error
$g(\sigma)$ = impulse response function
$i(t)$ = system input
$m(t)$ = system output
$r(t)$ = remnant
s = Laplace transform operator
$y_p(\sigma)$ = pilot impulse response function
τ = pilot reaction time delay
ω = frequency

Introduction

THE development of V/STOL and high-speed flight vehicles has brought about the problem that they are basically unstable or marginally controllable by the pilot in some phases of the flight. Stability augmentation systems are indispensable in order to obtain satisfactory vehicle characteristics. In case of stability augmentation failure, however, it becomes of the utmost importance to determine if the closed system consisting of the unstable vehicle and the human pilot can be stabilized to a certain extent. In view of this standpoint, the pilots' ability to accept marginal levels of static stability or damping, or both, has been a subject of discussion.

Several works, both theoretical and experimental, have so far been conducted to determine the controllability limit of the pilot in control of an unstable second-order system of Eq. (1).[1-5] Theoretical works treat the controllability limit in terms of stability limit or stability margin of the closed system, making assumptions on the pilot's transfer function form. Yet very few of the assumed transfer functions have been experimentally verified.

This report aims to investigate the propriety of the so far proposed controllability limit through the measurement of pilots' describing functions. A brief explanation is also made of an improved time domain analysis method to identify the describing function.

Problem Statement

Figure 1 shows the block diagram of the compensatory closed system under consideration. The transfer function of the controlled element is of the form

$$Y_c(s) = K_c/(s^2 + Xs + Y) \tag{1}$$

where K_c is a constant, and X and Y are the damping and static stability terms, respectively. The controlled element is unstable for negative values of X and/or Y. In Fig. 1, the human pilot is described in a quasi-linear form. $Y_p(s)$ is the linear model of the human pilot, which is to be identified, and $y_p(\sigma)$ the impulse response function of the linear model. The quantity $r(t)$, called remnant, is the portion of the pilot control output which is not linearly correlated with the system input $i(t)$.

In Fig. 2 are shown theoretically obtained controllability limits together with experimental results. It is also indicated in Fig. 2 that three kinds of instability are possible, depending upon the combination of (X, Y). In the region ①, the controlled element has two complex characteristic roots, and thus the dynamics are of oscillatory divergence. On the other hand, Eq. (1) has two positive real characteristic roots in the region ②, so that the response diverges quite quickly in an exponential manner. When the static stability is negative, namely in the region ③, the dynamics of the controlled element show the

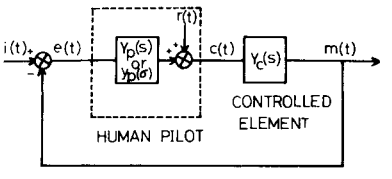

Fig. 1 Block diagram of a compensatory closed system.

Received June 26, 1973. The authors wish to thank Dr. Miyajima of Kawasaki Heavy Industries Inc. for his instructive advice. Mr. Tanaka of National Aerospace Laboratory is gratefully acknowledged for his cooperation in the experiment and his offer of the precious data.
Index categories: Aircraft Handling, Stability, and Control; VTOL Handling, Stability, and Control.

* Associate Professor, Department of Aeronautical Engineering.
† Professor, Department of Aeronautics.

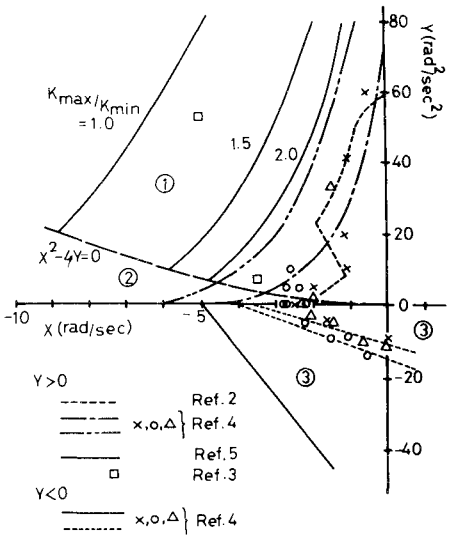

Fig. 2 Controllability limits.

instability similar to that of the first-order unstable element, since Eq. (1) in this region has one positive and one negative real root. Let us first discuss the controllability limit for positive static stability.

The dotted curve that has a switching line was obtained by Jex et al. under the assumption that the pilot employs two distinctly different modes, one purely compensatory and the other quasi-precognitive.[2] The pilot's transfer function used by them is of the following form

$$Y_p(s) = K_p e^{-\tau s}[s+(1/T_L)] \tag{2}$$

Chain lines are the controllability limits calculated by Washizu and Miyajima for two kinds of reaction time delay by the use of the pilot's transfer function of the form[4]

$$Y_p(s) = K_p e^{-\tau s}(1+T_L s)/(1+T_N s) \tag{3}$$

Meanwhile, Smith presented an experimental controllability limit, which is extremely high as shown in Fig. 2 by a □ mark.[3] It is hardly possible to explain this experimental result by the transfer function Eq. (2) or (3). The region in which □ is contained is ①, and thus the system response is quite oscillatory. Washizu and Miyajima considered that an experienced pilot could take notice of the existence of a periodicity of the response and could control it so that the periodically

Table 1 Input frequency components

i	a_i	ω_i rad/sec	i	a_i	ω_i rad/sec
1	a	0.262	1	a	0.157
2	$-a$	0.602	2	$-a$	0.262
3	a	1.49(ω_c)	3	a	0.419
4	$-0.1a$	4.03	4	$-a$	0.681
5	$0.1a$	13.8	5	a	0.995
			6	$-a$	1.78(ω_c)
			7	$0.1a$	2.78
			8	$-0.1a$	4.50
			9	$0.1a$	7.44
			10	$-0.1a$	11.7

a) $\sigma = 0.2$ cm

b) $\sigma = 0.87$ cm

$i(t) = \sum_{i=1}^{k} a_i \sin \omega_i t$: input

$\sigma^2 = \frac{1}{2}\sum_{i=1}^{k} a_i^2$: σ = rms amplitude of input

ω_c : cutoff frequency

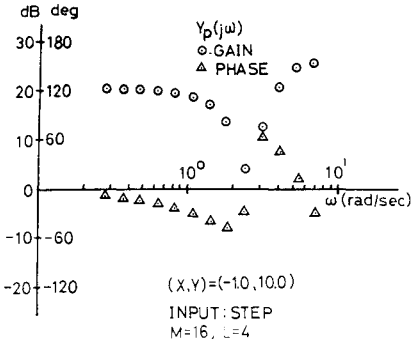

Fig. 3 Pilot describing function : average of 3 runs.

changing error would be cancelled out. In other words, the pilot who has been subjected to training can get the periodicity out of the given error signal and can apply control that has nearly 180° phase lead over the error signal.[5] Based on this consideration and on Smith's suggestion that the pilot is capable of generating a second-order lead term, they proposed a modified transfer function given below

$$Y_p(s) = K_p e^{-\tau s}\frac{1+T_L s+s^2/Y}{1+T_N s} \tag{4}$$

The first-order lead time constant, T_L, should be nonzero positive to attain closed-loop stability.

The controllability limit obtained by the closed-loop analysis through the use of Eq. (4) is shown in Fig. 2 by a solid curve. In the figure, K_{min} is the minimum open-loop gain required to make the system stable, and K_{max} the maximum open-loop gain beyond which the system becomes unstable again. Thus, it follows that the solid curve on which the parameter $K_{max}/K_{min} = 1$ gives the controllability limit. Note that the extremely high experimental result marked □ is included inside the controllability limit.

One of the objectives of this report is to determine if the human pilot is able to employ the transfer function of the form of Eq. (4) when he is engaged in the control of an unstable second-order system of oscillatory divergence.

As for the case of negative static stability, Washizu and Miyajima's result of closed-loop analysis through the use of Eqs. (1) and (3) shows distinct disagreement with their experimental results.[4] They state, in order to explain the disagreement, that the human pilot controls the unstable element by taking notice of the unstable root only. As the result, the controllability limit of the pilot in the region ③ is determined by the time to double amplitude of the unstable first-order mode, as shown by dotted lines in Fig. 2. This may suggest that in the region ③ the pilot will employ the transfer function which is similar to that for the unstable first-order system control. It is another objective of this report to measure the pilot's describing function in the region ③ and to compare that with the so far obtained experimental data associated with the first-order unstable system control.

Experiment

Fixed-base simulator tests were conducted. The simulator consists of an analog computer, an oscilloscope and a control stick with small inertia and without restoring spring. The system block diagram of the test is the same as shown in Fig. 1. The error, $e(t)$, was displayed on the oscilloscope by a horizontal bright segment moving vertically. The system input data used were a step of which the magnitude was 0.4 cm and a random appearing signal made up of a sum of sine waves, whose frequencies and rms value are listed in Table 1a. The random appearing signal was provided with a cutoff frequency, above which the amplitude of sine waves was set at one tenth that of the lower frequency sine waves. The cutoff frequency is also shown in Table 1a.

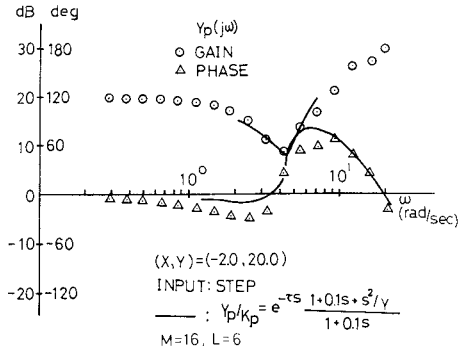

Fig. 4 Pilot describing function.

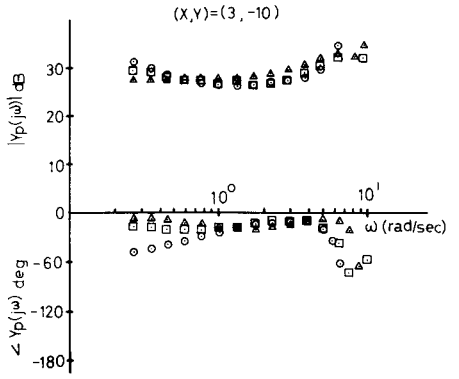

Fig. 6 Pilot describing functions: run to run variability.

Equation (1) is the transfer function of the controlled element. At tests, K_c was set equal to unity. Subjects were requested to minimize the error displayed on the oscilloscope to the best of their ability. Before data taking for a combination of (X, Y), each subject was trained up until the mean squared error, $\overline{e^2(t)}$, reached a nearly constant value. However, the system was judged to be uncontrollable, when the subject failed three times consecutively in keeping the bright segment within ± 4 cm for 30 sec. Describing functions obtained from this series of experiment are shown by Fig. 3 and Figs. 4–7.

Figure 8 is a result of a different series of experiments, where a few environmental conditions differ from those stated previously. The stick was equipped with a spring with the restoring force of 0.1 kg/cm. The frequencies of the random appearing signal used as the system input, the cutoff frequency, and rms value are as listed in Table 1b. The run length was 3 min for each run.

Of the results presented in this report, Figs. 3 and 4 are for a step input, and others are for random appearing inputs. Figures 3, 4, and 8 are results measured for the combination of (X, Y) in the region ①, and others, say Figs. 5–7, in the region ③.

Method of Analysis

Cross-spectral method or Fourier analysis method with the use of random or random appearing inputs is well developed and is usually used to identify the human pilot describing functions. These methods, however, have a disadvantage that relatively long data are required in order to obtain highly reliable results. For such a marginally controllable system as under consideration, it is often observed that the pilot's control behavior is quite nonlinear and/or nonstationary. As a result, much increase in remnant power is brought about to make the result less meaningful in the sense of identification of a linear model of the human pilot. As far as nonstationarity is concerned, it may be desirable to use data of shorter length during which the data can be regarded to be stationary. About nonlinear control behavior shown by the pilot in marginally controllable systems, some will be referred later.

A method that works with relatively short length of data is the time domain analysis method.[6] This method has been improved in this report so as to give more reliable results. A brief explanation is made below.

Consider the system of Fig. 9, where $G(j\omega)$ is the frequency response function of an unknown system and $g(\sigma)$, the impulse response function that corresponds to $G(j\omega)$. $G(j\omega)$ and $g(\sigma)$ are related by

$$G(j\omega) = \int_0^\infty g(\sigma)\, e^{-j\omega\sigma}\, d\sigma \tag{5}$$

In Fig. 9, the input to the unknown system is denoted by $x(t)$, and the actual output, which can be measured with an additive noise $n(t)$, by $y(t)$. The quantity $v(t)$, which is called residual or equation error, indicates the difference between the actual output $y(t)$ and the output of the linear model $z(t)$.

If the unknown system is the human pilot, we may equivalently consider, with reference to Fig. 1, that

$$G(j\omega) = Y_p(j\omega) \tag{6a}$$
$$g(\sigma) = y_p(\sigma) \tag{6b}$$
$$x(t) = e(t) \tag{6c}$$
$$y(t) = c(t) \tag{6d}$$

It is possible to estimate $Y_p(j\omega)$ by setting as abovementioned through the least square method described later in this section. However, when the system is operating in a closed-loop fashion

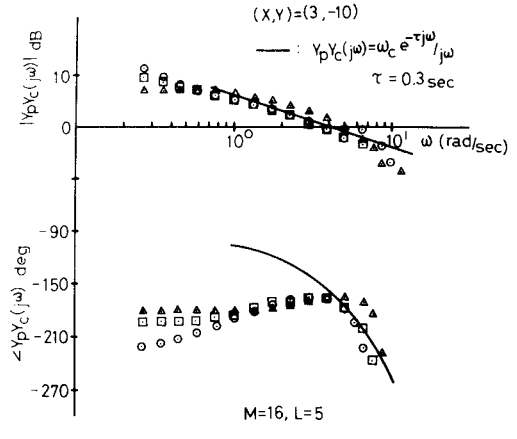

Fig. 5 Open-loop describing functions: run to run variability.

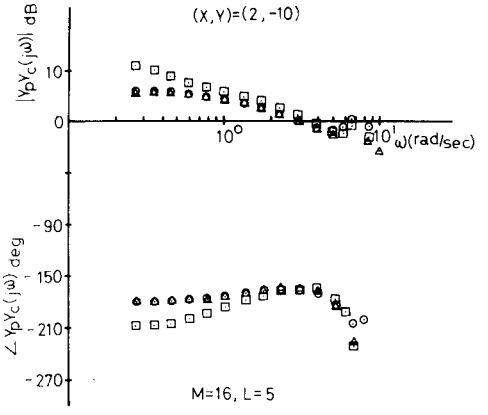

Fig. 7 Open-loop describing functions: run to run variability.

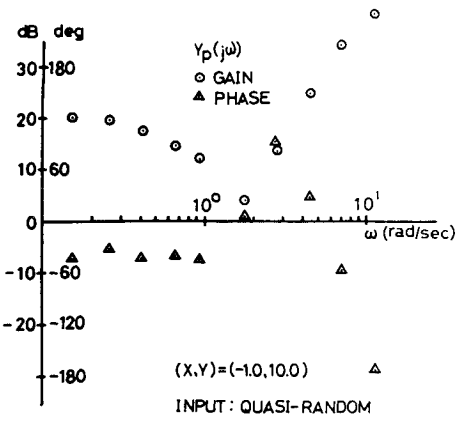

Fig. 8 Pilot describing function : average of 10 runs.

as in Fig. 1, the error, $e(t)$, contains the portion that has no linear correlation with the input. This input-uncorrelated portion causes harmful effect such as bias on the estimation of the linear model. It may be better to set $x(t) = i(t)$ as the system input and $y(t) = m(t)$ as the system output, since the linear correlation with the system input is important. Then, we shall obtain the closed-loop describing function, $G(j\omega)$, related by Eq. (7) to the pilot describing function, $Y_p(j\omega)$, and the controlled element frequency response function, $Y_c(j\omega)$

$$G(j\omega) = Y_p Y_c(j\omega)/[1 + Y_p Y_c(j\omega)] \tag{7}$$

Once the impulse response function, $g(\sigma)$, is found, $G(j\omega)$ is given by Eq. (5) and the pilot describing function is finally calculated from Eq. (7), since $Y_c(j\omega)$ is a priori known.

With reference to Fig. 9, $x(t)$ and $y(t)$ are related by

$$\begin{aligned} y(t) &= z(t) + v(t) \\ &= \int_0^{T_M} g(\sigma)x(t-\sigma)\,d\sigma + v(t) \end{aligned} \tag{8}$$

where it is assumed that

$$g(\sigma) = 0 \qquad \sigma > T_M \tag{9}$$

Direct estimation of the impulse response function, $g(\sigma)$, is possible from Eq. (8) through the use of the least square method. Previous works on the least square method, however, state that the estimated $g(\sigma)$ is biased unless the process $v(t)$ is uncorrelated.[8] In order to get rid of the bias, a filter of Eq. (10) to prewhiten the process $v(t)$ is used

$$\varepsilon(t) = \int_0^T h(\sigma')v(t-\sigma')\,d\sigma' \tag{10}$$

In Eq. (10), $h(\sigma')$ is the impulse response function of the prewhitening filter, and it is assumed that

$$h(\sigma') = 0 \qquad \sigma' > T \tag{11}$$

The operation of prewhitening, Eq. (10), on Eq. (8) yields the following

$$y^*(t) = z^*(t) + \varepsilon(t) \tag{12}$$

where

$$y^*(t) = \int_0^T h(\sigma')y(t-\sigma')\,d\sigma' \tag{13a}$$

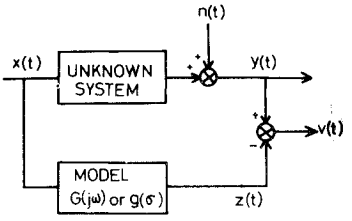

Fig. 9 Block diagram of impulse response estimation.

$$z^*(t) = \int_0^T h(\sigma')z(t-\sigma')\,d\sigma' \tag{13b}$$

and

$$z(t) = \int_0^{T_M} g(\sigma)x(t-\sigma)\,d\sigma \tag{13c}$$

For analysis, it is more appropriate to write Eqs. (8–11) in sampled data form as

$$y(n) = \sum_{m=1}^{M} \bar{g}(m)x(n-m+1) + v(n) \tag{8b}$$

$$\bar{g}(m) = 0 \qquad m > M \tag{9b}$$

$$\varepsilon(n) = -\sum_{l=0}^{L} \bar{h}(l)v(n-l) \tag{10b}$$

$$\bar{h}(l) = 0 \qquad l > L \tag{11b}$$

where

$$\bar{g}(m) = g(m) \cdot \Delta \tag{14}$$

$$\bar{h}(l) = -h(l) \cdot \Delta \tag{15}$$

and Δ is the sampling interval. In addition

$$n = M,\ M+1, \cdots\cdots, N \tag{16}$$

and l, m, n, M, and N are integers. T_M, T, and the data length T_D are related to M, L, and N, respectively, as

$$T_M = (M-1) \cdot \Delta \tag{17a}$$

$$T = L \cdot \Delta \tag{17b}$$

$$T_D = (N-1) \cdot \Delta \tag{17c}$$

Equation (10) can be reduced to the following autoregressive form, if $\bar{h}(0)$ is selected such that $-\bar{h}(0) = 1$

$$v(n) = \sum_{l=1}^{L} \bar{h}(l)v(n-l) + \varepsilon(n) \tag{18}$$

In Eq. (18), $\{\varepsilon(n)\}$ is a sequence of uncorrelated random variables.

Equation (12) can also be expressed in the sampled data form as follows: if Eqs. (9b) and (11b) are taken into account and the prewhitening filter of the form of Eq. (18) is used[7]

$$y(n) = \sum_{l=1}^{L} \bar{h}(l)y(n-l) + \sum_{m=1}^{M+L} \alpha(m)x(n-m+1) + \varepsilon(n) \tag{19}$$

where

$$\alpha(m) = \bar{g}(m) - \sum_{l=1}^{m} \bar{h}(l)\bar{g}(m-l) \tag{20}$$

In matrix form, Eq. (19) reduces to

$$\bar{y} = \Phi\bar{\beta} + \bar{\varepsilon} \tag{21}$$

where

$$\bar{y}^T = [y(M)y(M+1) \cdots\cdots y(N)] \tag{22}$$

$$\bar{\varepsilon}^T = [\varepsilon(M)\varepsilon(M+1) \cdots\cdots \varepsilon(N)] \tag{23}$$

$$\bar{\beta}^T = [\bar{h}(1)\bar{h}(2) \cdots \bar{h}(L) : \alpha(1)\alpha(2) \cdots \alpha(M+L)] \tag{24}$$

and

$$\Phi = \begin{bmatrix} y(M-1)\ y(M-2) \cdots y(M-L) & : & x(M) & x(M-1) \cdots x(1)\ 0 \cdots\cdots 0 \\ y(M) \cdots\cdots y(M-L+1) & : & x(M+1) & x(M) \cdots\cdots x(2)\ x(1) 0 \cdots\cdots 0 \\ \vdots \qquad\qquad \vdots & & \vdots & \vdots \qquad\qquad\qquad \vdots \\ y(M+L-1) \cdots\cdots y(M) & : & x(M+L) & x(M+L-1) \cdots\cdots x(1) \\ \vdots \qquad\qquad \vdots & & \vdots & \vdots \qquad\qquad\qquad \vdots \\ y(N-1) \cdots\cdots \cdots y(N-L) & : & x(N) & x(N-1) \cdots\cdots x(N-M-L+1) \end{bmatrix} \tag{25}$$

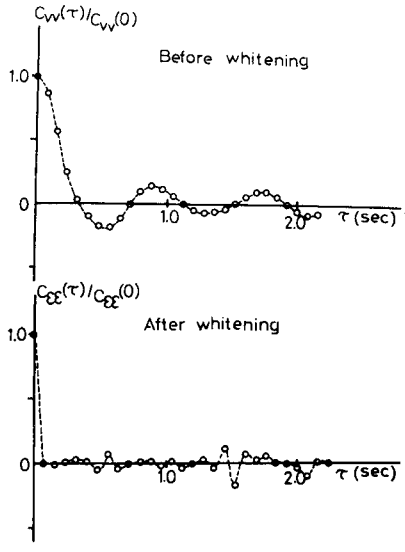

Fig. 10 Correlation functions of residuals before whitening and after whitening.

The unknown parameter vector $\bar{\beta}$ is estimated by minimizing the cost function

$$J = [\bar{y} - \Phi\bar{\beta}]^T[\bar{y} - \Phi\bar{\beta}] \tag{26}$$

Thus, the estimated parameter vector $\hat{\bar{\beta}}$ is given by

$$\hat{\bar{\beta}} = [\Phi^T\Phi]^{-1}\Phi^T\bar{y} \tag{27}$$

The cost J is also a function of the order of the impulse response M and that of the prewhitening filter L. Therefore, it is desired to test if the reduction of the cost function is significant when M and L are increased one by one. Values of M and L used to obtain the results presented in this report are shown in each figure. Figure 10 is an example that shows how the prewhitening filter of Eq. (18) works to whiten the sequence $\{v(n)\}$. In the figure, C_{vv} and $C_{\varepsilon\varepsilon}$ are the autocorrelation functions of $v(t)$ and $\varepsilon(t)$, respectively. Values of the data length T_D and the sampling interval used for the analysis were 27.0 sec and 0.1 sec, respectively.

All results in this report except for Fig. 8 were analyzed by the improved time domain method. Figure 8 is one of rare cases where the Fourier analysis technique worked successfully. When a sum of sine waves is used as the system input, the human pilot's describing function, $Y_p(j\omega)$, is able to be identified as

$$Y_p(j\omega_i) = C(j\omega_i)/E(j\omega_i) \tag{28}$$

where with reference to Fig. 1, $C(j\omega_i)$ and $E(j\omega_i)$ are Fourier transforms of $c(t)$ and $e(t)$, respectively, computed at the input frequency ω_i. In applying Eq. (28), it is assumed that the effect of remnant on $C(j\omega_i)$ and $E(j\omega_i)$ is small. If the remnant power is actually so large as to make it impossible to discriminate between linear response to the input and the remnant, the identification by Eq. (28) sometimes yields the result that $Y_p(j\omega) \sim -1/Y_c(j\omega)$.

Discussion on Results

Figure 11 is an example of the Bode diagram of Eq. (4) depicted for the dimensionless static stability $\tau^2 Y = 0.2$. The abscissa of Fig. 11 is dimensionless frequency, $\tau\omega$. Since Eq. (4) is applicable only to the system of oscillatory divergence (i.e., the region ① in Fig. 2), experimental results, Figs. 3, 4, and 8 are discussed with reference to Fig. 11.

Notice that the Bode diagram of Fig. 11 shows a peculiar feature at the frequency $\tau\omega = \tau(Y)^{1/2}$. For a small T_L (the first-order lead time constant) the gain takes small value and the phase shows nearly 180° change at $\tau\omega = \tau(Y)^{1/2}$. It is of interest to compare Fig. 11 with the frequency characteristics of the controlled element, Eq. (1). The controlled element is apt to intensify the frequency component around $(Y)^{1/2}$ rad/sec. On the other hand, the pilot expressed by Eq. (4) suppresses the frequency component around $(Y)^{1/2}$ rad/sec, which is considered to be dominant in the response.

Looking at Figs. 3 and 4 that show step input describing functions, the similarity of the curves between these and Fig. 11 will be clear. Figure 4 is for the static stability Y of 20.0 rad^2/sec^2; if τ is assumed to be 0.1 sec, the curve in Fig. 11 for T_L of 0.1 sec ($T_L/\tau = 1.0$) fits well as shown by solid lines in Fig. 4. T_N, the neuromuscular lag time constant, is assumed here to be equal to τ.

Figure 8 is a result for a random appearing input and for the same combination of (X, Y) as Fig. 3. Comparing Fig. 8 with Fig. 3 may suggest that the pilot's transfer function of the form of Eq. (4) is applicable to both step input and random appearing input cases. The gain minimum frequency ($\tau\omega = \tau(Y)^{1/2}$ in Fig. 11) seems to become a bit lower than the expected value of $(Y)^{1/2}$ rad/sec as the static stability decreases.

For the results presented thus far, rather small values of T_L seem to be appropriate to fit Eq. (4). However, some of the data we have obtained show that rather large values of T_L, somewhat between 0.2 sec and 0.3 sec, are sometimes employed by the pilot.

From these experimental results, it may be concluded that the pilot is able to adopt the transfer function of Eq. (4) when he controls the dynamically unstable system of Eq. (1).

Now we proceed to the negative static stability case (the region ③ in Fig. 2). In Fig. 5 is shown the open-loop describing function and in Fig. 6 the pilot's describing function for $(X, Y) = (3.0, -10.0)$. Figure 5 reminds us of the cross-over model that claims that the open-loop describing function takes the form of Eq. (29) around the cross-over frequency, ω_c

$$Y_p\, Y_c(j\omega) = \omega_c\, e^{-\tau j\omega}/j\omega \tag{29}$$

Solid lines in Fig. 5 are the curves fitted to the experimental data according to Eq. (29). The cross-over frequency selected for the fitting is that of the average of three runs shown in Fig. 5. Low-frequency phase difference between the experimental data and the solid curve could be compensated for if the α term, which is interpreted as the midfrequency effects of the low-frequency phase droop,[10] is added to have the following open-loop describing function form

$$Y_p\, Y_c(j\omega) = \omega_c \frac{e^{-j[\tau\omega + (\alpha/\omega)]}}{j\omega} \tag{30}$$

It can be observed in Fig. 6 that the pilot gain is almost constant over the midfrequency region. Also taking into account the phase tendency suggests that the pilot's describing function for this combination of (X, Y) is expressed approximately by

$$Y_p(j\omega) = K_p\, e^{-\tau j\omega} \tag{31}$$

Reference 10 contains a number of describing function data for the pilot's control of unstable first-order systems. The un-

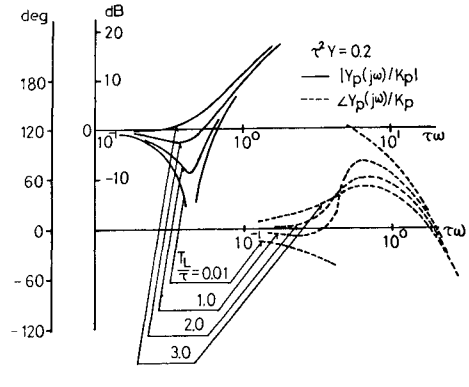

Fig. 11 Theoretical frequency response of the pilot controlling an unstable system of oscillatory divergence.

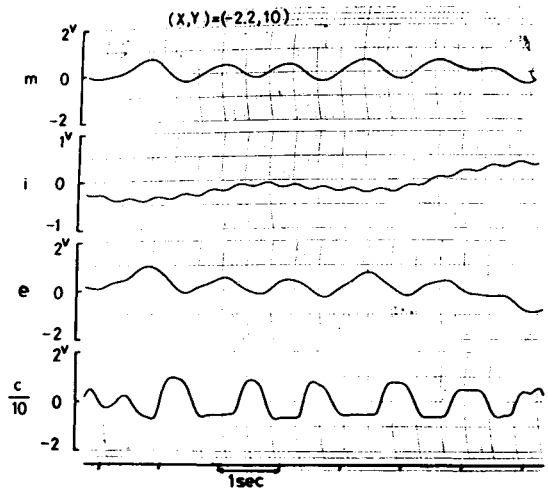

Fig. 12 An example of the pilot's bang-bang type control.

stable characteristic root of the statically unstable second-order system used to obtain Figs. 5 and 6 is 2.0 rad/sec. The describing function data in Ref. 10 for the same unstable first-order mode (gain level of the controlled element is different) show much similarity to Figs. 5 and 6, although difference in the cross-over frequency is resulted from difference in subjects and inputs. The rising data points at either end in Fig. 6 (which are also noticed in Ref. 10) are, as Ref. 10 states, due to intrinsic neuromuscular characteristics of the pilot but are not due to any equalization.

Figure 7 is the result for a more difficult system. It can be seen that the pilot well matches the cross-over model. These results may allow us to conclude that the pilot controls the system of Eq. (1) with negative static stability as if he were controlling a first-order unstable system, paying attention only to the unstable real characteristic root. This may explain that in Ref. 4 the controllability limit for negative static stability is closely associated with the time to double amplitude of the unstable characteristic root. Note, however, that if the pilot is able to make lead equalization, the controllability limit becomes wider.

A few remarks are to be added to the preceding discussion. The first one is about the effect of input power on the pilot describing function. During a series of experimental runs to obtain the describing functions presented in this report, the input power (or the mean square amplitude of the input) was set constant. However, seeing to it that the pilot describing function is dependent upon input, it is worthwhile to study the effect of input power level. We have conducted another series of experiments, where several quasi-random inputs (sum of sine waves) of different power levels but of same frequency components are used. The controlled element is Eq. (1) of oscillatory divergence. The results of this series of experiment are not yet satisfactorily definite, but the essentials can be itemized as follows:

1) When the power level of the input is small, the pilot pays attention to the periodicity due to the controlled element dynamics, so that his describing function takes the form of Eq. (4), and the second-order lead time constant is approximately equal to $1/Y$ sec^2.

2) As the input power level becomes larger, the pilot is likely to share his attention between the frequency component associated with the controlled element dynamics and the predominant frequency in the input. As a result, the gain minimum frequency is not necessarily equal to $(Y)^{1/2}$ rad/sec.

3) When the input power level is very large, the pilot is not able to grasp the periodicity due to the controlled element dynamics. The pilot's control manner and the describing function are largely influenced by the input frequency.

Another remark is made of the nonlinear control behavior exhibited by the pilot. The pilot's control output often shows quite clear nonlinearity when the controlled element dynamics reach his controllability limit. An example of such nonlinear control is shown in Fig. 12, where the pilot's control looks like bang-bang type. Bang-bang type or pulse type control is also exhibited by the pilot when he controls high order systems.[11] It is yet unknown whether or not such nonlinear control helps widen the controllability limit. It is one of the tasks for the future to make clear the nonlinear control behavior shown by the pilot.

Conclusion

Human pilots' describing functions, when controlling unstable second-order systems, have been measured. When the system is of oscillatory divergence or dynamically unstable, the practiced pilot pays special attention to the periodicity of the error signal and tries to cancel the dominant periodic component, adopting the describing function of Eq. (4) that contains a second-order lead term.

For the negative static stability case, pilots' control behavior is very similar to that shown when they control first-order unstable systems. The pilot's concern is to suppress the response from the unstable real characteristic root.

In this report no data of describing functions in the region ② of Fig. 2 are presented at all. This is because the controlled element of Eq. (1) in this region is hardly controllable by pilots, and few data have been obtained yet.

References

[1] Taylor, L. W. and Day, R. E., "Flight Controllability Limit and Related Human Transfer Functions as Determined from Simulator and Flight Tests," TN-D 746, May 1961, NASA.

[2] Jex, H. R., Cromwell, C. H., and Siskind, R. K., "Correlation of Experimental and Theoretical Limits for Pilot Control of Unstable Second-Order Systems," TM-56, July 1960, Systems Technology Inc., Inglewood, Calif. (unpublished).

[3] Smith, R. H., "On the Limits of Manual Control," *IEEE Transactions on Human Factors in Electronics*, Vol. HFE-4, Sept. 1963, pp. 56–59.

[4] Washizu, K. and Miyajima, K., "Controllability Limit of a Human Pilot," *AIAA Journal*, Vol. 3, No. 5, May 1965, pp. 941–947.

[5] Washizu, K. and Miyajima, K., "Some Consideration on the Controllability Limit of a Human Pilot," *AIAA Journal*, Vol. 5, No. 1, Jan. 1967, pp. 151–155.

[6] Taylor, L. W., Jr., "Nonlinear Time Domain Models of Human Controllers," NASA SP-215, March 1969.

[7] Akaike, H., "On the Use of a Linear Model for the Identification of Feedback Systems," *Ann. Inst. Statist. Math.*, Vol. 20, 1968, pp. 425–439.

[8] Åström, K. J. and Eykhoff, P., "System Identification—A Survey," *Automatica*, Vol. 7, Pergamon Press, New York, 1971, pp. 123–162.

[9] Goto, N. and Endo, S., "Manual Control of an Oscillatory Divergent System," *Transactions of the Japan Society for Aeronautical and Space Sciences*, Vol. 16, No. 32, 1973, pp. 129–140.

[10] Jex, H. R., McDonell, J. D., and Phatak, A. V., "A 'Critical' Tracking Task for Man-Machine Research Related to the Operator's Effective Delay Time—I: Theory and Experiments with a First-Order Divergent Controlled Element," CR-616, Oct. 1966, NASA.

[11] Young, L. R. and Meiry, J. L., "Bang-Bang Aspects of Manual Control in High-Order Systems," *IEEE Transactions on Automatic Control*, Vol. AC-10, June 1965, pp. 336–341.